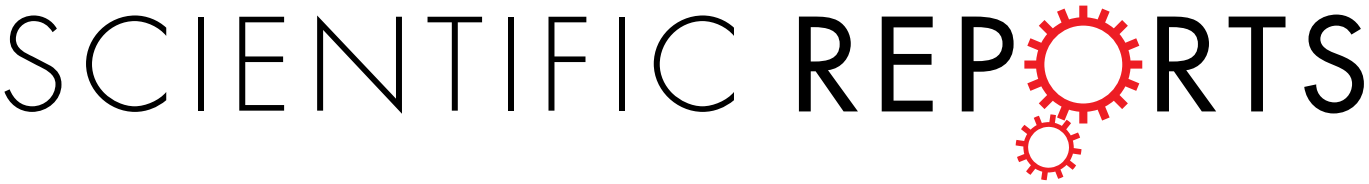

OPEN

# Vacancy-induced brittle to ductile transition of W-M co-doped $Al_3Ti$ (M=Si, Ge, Sn and Pb)

Received: 27 April 2017
Accepted: 9 October 2017
Published online: 25 October 2017

Mingke Zhu[1,2], Ping Wu[3], Qiulin Li[2] & Ben Xu[1]

**We investigated the effect of vacancy formation on brittle ($D0_{22}$) to ductile ($L1_2$-like) transition in $Al_3Ti$ using DFT calculations. The well-known pseudogap on the density of states of $Al_3Ti$ migrates towards its Fermi level from far above, via a W — M co-doping strategy, where M is Si, Ge, Sn or Pb respectively. In particular, by a W — M co-doping the underline electronic structure of the pseudogap approaches an octahedral ($L1_2$: $t_{2g}$, $e_g$) from the tetragonal ($D0_{22}$: $e_g$, $b_{2g}$, $a_{1g}$, $b_{1g}$) crystal field. Our calculations demonstrated that (1) a W-doping is responsible for the close up of the energy gap between $a_{1g}$ and $b_{1g}$ so that they tend to merge into an $e_g$ symmetry, and (2) all M-doping lead to a narrower gap between $e_g$ and $b_{2g}$ (moving towards a $t_{2g}$ symmetry). Thus, a brittle to ductile transition in $Al_3Ti$ is possible by adopting this W — M co-doping strategy. We further recommend the use of W-Pb co-doped $Al_3Ti$ to replace the less anodic Al electrode in Al-battery, due to its improved ductility and high Al diffusivity. Finally this study opens a new field in physics to tailor mechanical properties by manipulating electron energy level(s) towards higher symmetry via vacancy optimization.**

Brittle to ductile transition is of interest to a wide range of fundamental research and applications[1–6]. In particular, effects of either intrinsic vacancy[7,8], extra-electron[9], or dopants[10,12] on brittle-ductile transition in $Nb_5Si_3$, NiSc, $Al_{12}W$-type and $L1_2$-$Al_3Sc$ are reported. TiAl-based intermetallic compounds are desirable candidates for high temperature structural applications due to many attractive properties. Among the Al-Ti alloys, $Al_3Ti$ has received particular interests for its high specific strength, elastic moduli[13], low density (~3.3 g/cm$^3$), good thermal conductivity and high melting point (~1400 °C). However, the stable but brittle tetragonal $D0_{22}$-$Al_3Ti$ is less favored in real applications. Many investigations are conducted aiming to improve the ductility of $D0_{22}$-$Al_3Ti$. Hong[12] calculated the density of states (DOS) of the brittle $D0_{22}$-$Al_3Ti$ and the ductile $L1_2$-$Al_3Ti$ phases, and proposed a strategy to simultaneously stabilize the ductile $L1_2$ and destabilized the brittle $D0_{22}$ phase by ternary alloy additions. He further pointed out that by adding in lower-valence elements, the pseudogap (on DOS) migrates from above to below the Fermi level, thus, diminishing simultaneously the antibonding for the ductile $L1_2$ and the bonding states for the brittle $D0_{22}$ phases. But Hong did not take into consideration the formation of either intrinsic or extrinsic defects into his model. On the other hand, Niu[9] proposed to promote ductile to brittle transitions in $Al_{12}W$-type intermetallic by an extra-electron doping, which is on the opposite direction of the current work. The underline electronic structures of pseudogap in both $D0_{22}$ and $L1_2$ $Al_3Ti$ phases are reported recently by Chen[14]. Crystal field splitting as shown in Fig. 1 is found responsible for the formation of the pseudogaps, i.e., an octahedral crystal field of $e_g$ ($d^2_{x-y}$, $d^2_z$) and $t_{2g}$ ($d_{xy}$, $d_{xz}$, $d_{yz}$) for the ductile $L1_2$ phase, and a tetragonal one of $b_{1g}$ ($d^2_{x-y}$), $a_{1g}$ ($d^2_z$), $b_{2g}$ ($d_{xy}$) and $e_g$ ($d_{xy}$, $d_{yz}$) for the brittle $D0_{22}$ phase. It is interesting to notice that the main difference between the octahedral and tetragonal crystal field splitting is the elongation in tetragonal along the z-axis, which relaxes the electron density along the z-axis and moves (1) the $d^2_z$ energy downwards apart from the $d^2_{x-y}$ and (2) the $d_{xz}$ and $d_{yz}$ lower than the $d_{xy}$ level. An effective unit area as shown in Fig. 2a is defined as $S = l_x \times l_y$, where $l_x$ and $l_y$ is respectively the shortest atomic distance along the x and y axis. By shrinking the unit cell (or d in Fig. 2a) along the z-axis or expanding in the xy-plane indicated by S, a tetragonal crystal structure may return to and approach an octahedral-like structure. Thus, by reducing the ratio $r$ (Å$^{-1}$) ($r = d/S$), a brittle-ductile transition may be facilitated. From first-principles calculations, we test this new strategy to achieve the designed reduction of $r$ by adopting a W — M co-doping strategy. Key challenges in this approach are (1) to generate sufficient Al

[1]School of Materials Science and Engineering, Tsinghua University, Beijing, 100084, P. R. China. [2]Graduate School at Shenzhen, Tsinghua University, Shenzhen, 518055, P. R. China. [3]Singapore University of Technology and Design, 487372, Singapore, Singapore. Correspondence and requests for materials should be addressed to P.W. (email: wuping@sutd.edu.sg) or Q.L. (email: liql@sz.tsinghua.edu.cn)

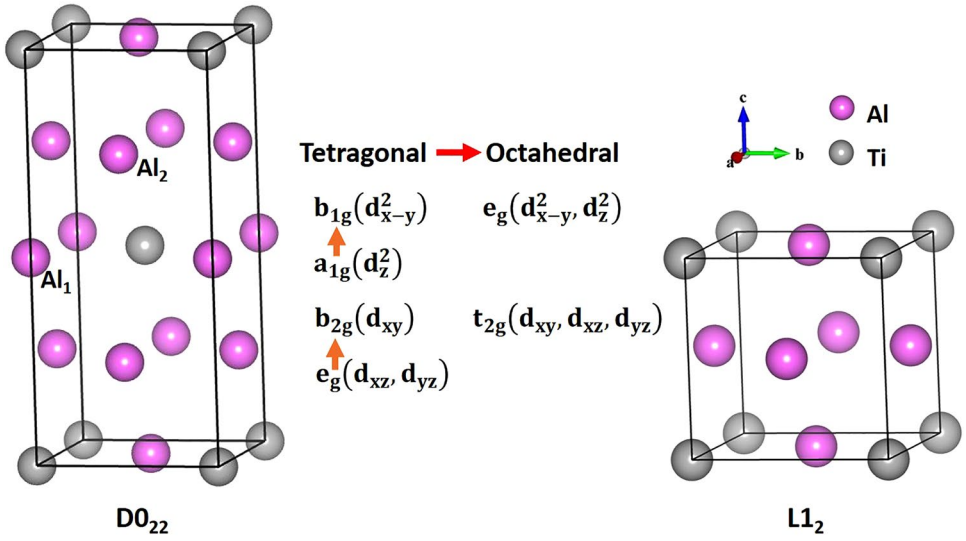


**Figure 1.** Comparison of the lattice and electronic structures between $D0_{22}$-$Al_3Ti$ and $L1_2$-$Al_3Ti$. The schematic diagram between the two structures shows that for the tetragonal $D0_{22}$-$Al_3Ti$, the 3*d*-orbital splits into $b_{1g}$ ($d^2_{x-y}$), $a_{1g}$ ($d^2_z$), $b_{2g}$ ($d_{xy}$) and $e_g$ ($d_{xy}$, $d_{yz}$), while for the octahedral $L1_2$-$Al_3Ti$, the 3*d*-orbital splits into $e_g$ ($d^2_{x-y}$, $d^2_z$) and $t_{2g}$ ($d_{xy}$, $d_{xz}$, $d_{yz}$).

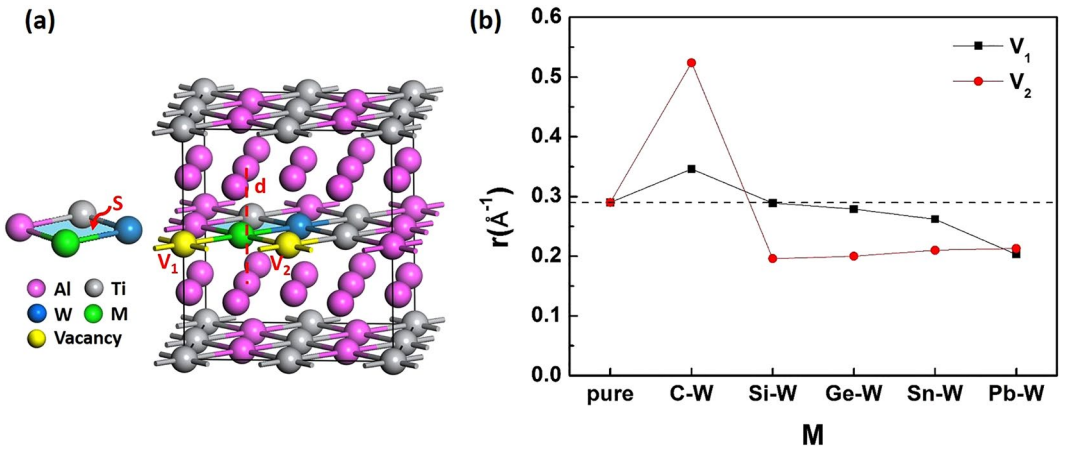


**Figure 2.** (**a**) Crystal structure of the W − M co-doping $Al_3Ti$ (Note that the unit cell length (**d**) along the z-axis and the effective unit area (S) are highlighted, where $l_x$ is the length between M and Ti and $l_y$ is the length between Al and W). (**b**) The calculated ratio $r$ (Å$^{-1}$) ($r = d/S$) in pure $D0_{22}$-$Al_3Ti$ and W − M co-doping systems with an Al vacancy at the $V_1$ site.

vacancies in $D0_{22}$-$Al_3Ti$ to make the brittle structure more deformable and (2) to manipulate specific electron energy levels to transfer the low symmetry tetragonal to a high symmetry octahedral-like crystal field.

Moreover, due to the decrease in Gibbs free energy, $Al_3Ti$ may also be used as the anode material to replace Al in Al-battery. Recently, electronic structure of pure $D0_{22}$-$Al_3Ti$[12,14] and Al diffusion mechanisms of $D0_{22}$-$Al_3Sc$[11] are reported. However, like many brittle intermetallics, short cycling life of a native $D0_{22}$-$Al_3Ti$ electrode is expected due to the structure damages during the charge and discharge processes. In addition, high Al diffusivity is essential to Al-battery, which requires an easy formation of Al vacancy based on Shi's[11] findings that Al vacancies facilitate the Al diffusion in $Al_3Sc$. Therefore, the current study on the formation of Al vacancies may provide practical solutions to enhance both the mechanical and electrochemical properties of $Al_3Ti$ for Al-battery applications.

## Results

**Crystal structure.** Crystal structures of both the ductile ($L1_2$) and brittle ($D0_{22}$) phases are shown in the Fig. 1. A $L1_2$-$Al_3Ti$ crystallizes in the $Pm\bar{3}m$ space group, in which the Al atoms are located at the face centers of the cubic lattice and the Ti atoms are located at the vertices. And a $D0_{22}$-$Al_3Ti$ crystallizes in the *I4/mmm*. The conventional $D0_{22}$ cell contains two Al atoms at the Wyckoff site 2b (defined as $Al_1$), four Al atoms at the 4d site (defined as $Al_2$) and two Ti atoms at the 2a site. In this study, the lattice parameters are fixed at the values of

| M | C | Si | Ge | Sn | Pb |
|---|---|---|---|---|---|
| $E_M$(eV) | −160.52 | −160.49 | −159.85 | −157.87 | −156.90 |
| $E_{W-M}$(eV) | −169.87 | −168.69 | −167.85 | −165.79 | −164.62 |
| $\Delta E$ | 1.945 | 0.795 | 0.595 | 0.515 | 0.315 |

**Table 1.** The total energies of M doping $Al_3Ti$ ($E_M$) and W − M co-doping $Al_3Ti$ ($E_{W-M}$), and $\Delta E$.

a = b = 0.3851 nm and c = 0.8611 nm, for c/a = 2.236, which are in satisfactory agreement with other experimental and calculation results[15,16].

To conduct a systematic study, the site preference of W in $D0_{22}$-$Al_3Ti$ was investigated first by using a $2 \times 2 \times 1$ supercell including 32 atoms. The first-principles calculations have been performed to calculated the total energies $E_{tot}$ for the pure $D0_{22}$-$Al_3Ti$ supercell and $E_{dope}$ for [$(Al_{23}W)Ti_8$] and [$Al_{24}(Ti_7W)$] structures. To determine the site preference of W, the substitution energy $E_{sub}$ is defined as:

$$E_{sub} = E_{dope} - E_{tot} + \mu_{Al/Ti} - \mu_W \quad (1)$$

where $\mu_i$ (i = Al, Ti and W) is the chemical potential of these atoms in their stable bulk phases. In this study, the stable phases are considered as Ti in *hcp* structure[17], Al in the *fcc* structure[18]. After occupying $Al_1$, $Al_2$ and Ti site by a W-atom, the substitution energies of the three structures are −1.089 eV, −0.969 eV and 0.005 eV, respectively. It is clearly seen that the ternary W-atom strongly favors the Al site over the Ti site in the $D0_{22}$-$Al_3Ti$. Therefore, we default to substitute W-atom at the $Al_1$ site in the following work, as the blue sphere shown in Fig. 2a.

Then the IV-group elements M (M = C, Si, Ge, Sn and Pb) were introduced into the $D0_{22}$-$Al_3Ti$/W system and occupied the Ti site to form a W − M cluster, as the green sphere shown in Fig. 2a. The substitution energies of single M-atom doping at the Ti site in $D0_{22}$-$Al_3Ti$ can be written as:

$$E_{sub}(M) = E_M - E_{tot} + \mu_{Ti} - \mu_M \quad (2)$$

where $E_M$ is the total energy of single M-atom occupying Ti site. While the substitution energies of W − M clusters can be written as:

$$E_{sub}(W - M) = E_{W-M} - E_{tot} + \mu_{Al} + \mu_{Ti} - \mu_W - \mu_M \quad (3)$$

where $E_{w-M}$ is the total energy of W − M co-doping system. $\Delta E$ is defined as:

$$\begin{aligned} \Delta E &= E_{sub}(M) - E_{sub}(W - M) \\ &= E_M - E_{W-M} - \mu_{Al} + \mu_W \end{aligned} \quad (4)$$

The results are showed in Table 1. $\Delta E$ are positive which means that the co-doping systems have much lower substitution energies than the single doping systems. It indicates that introducing W in pure $D0_{22}$-$Al_3Ti$ structure will conduce to the substitution of Ti by M.

**Vacancy formation energy.** The crystal model with an Al vacancy were created by removing an individual Al-atom from W − M co-doping supercell. In order to reduce the computation loads, we focus on the first-nearest neighbors, thus, the two possible Al vacancies are at $V_1$ and $V_2$ sites considering the system symmetry, shown as yellow spheres in Fig. 2a. The stability of the defected structures were studied by vacancy formation energy calculation after the atomic defects are relaxed completely. The formation energy of a neutral aluminum vacancy (hereafter simply referred to as an aluminum vacancy) ($E_V$) is estimated by the following equation (5):

$$E_V(M) = E_{def} - E_{W-M} + \sum_i n_i \mu_i \quad (5)$$

where $E_V(M)$ is the vacancy formation energy, $E_{def}$ is the total energy of $D0_{22}$-$Al_3Ti$/W supercell containing one M-atom and one Al vacancy simultaneously and $E_{W-M}$ is the total energy of W − M co-doping supercell. The last term represents the difference in the number of atoms from the W − M co-doping system, where $n_i$ denotes the number of atoms to be taken from or inserted into the supercell in order to take account of point defect generation. If a corresponding atom is inserted into the supercell, $n_i$ is negative and if such an atom is taken away from the supercell, $n_i$ is positive. $\mu_i$ is the chemical potential of these atoms in their stable bulk phases. The calculated defect formation energies are tabulated in Table 2.

From Table 2, it can be easily observed that the vacancy formation energies of Al at $V_1$ site are higher than that at $V_2$ site. For a W − M co-doping system, when the Al vacancy occurs at $V_2$ site, the vacancy formation energies are negative under both Al-rich environment and Ti-rich environment, which indicates $V_2$ defects can be formed spontaneously during the fabrication of the alloy. In addition, both $V_1$ and $V_2$ defects are spontaneously formed by a W-Pb co-doping under either Al-rich or Ti-rich environment. The results attribute to the fact that the W − M co-doping cluster plays a vital role in the formation of Al vacancies.

**Electronic states of defected structure.** The calculated DOS are given in Fig. 3a for the pure $D0_{22}$-$Al_3Ti$, and in Fig. 3b–f for W-C, W-Si, W-Ge, W-Sn and W-Pb co-doping $Al_3Ti$ with an Al vacancy at the $V_1$ site, respectively. $\Delta n$ is introduced to indicate the valley of psuedogap. The value of $\Delta n$ is the energy of the lowest position on the calculated DOS curve. Thus, the positive value means the psuedogap is higher than the Fermi

| | $E_{V_1}$(eV) | | $E_{V_2}$(eV) | |
|---|---|---|---|---|
| | **Al-rich** | **Ti-rich** | **Al-rich** | **Ti-rich** |
| W-C | 2.00 | 1.47 | −0.08 | −0.61 |
| W-Si | 1.15 | 0.62 | −0.07 | −0.59 |
| W-Ge | 0.95 | 0.43 | −0.14 | −0.67 |
| W-Sn | 0.42 | −0.11 | −0.41 | −0.94 |
| W-Pb | −0.59 | −1.11 | −0.59 | −1.05 |

**Table 2.** The vacancy formation energies of W − M co-doping $Al_3Ti$ when an Al vacancy forms at $V_1$ site ($E_{V_1}$) or $V_2$ site ($E_{V_2}$) under both Al-rich and Ti-rich environment.

| | **pure $Al_3Ti$** | **C** | **Si** | **Ge** | **Sn** | **Pb** |
|---|---|---|---|---|---|---|
| $\Delta n$(eV) | 0.876 | 0.798 | 0.684 | 0.678 | 0.587 | 0.125 |

**Table 3.** The position of the valley of psuedogap.

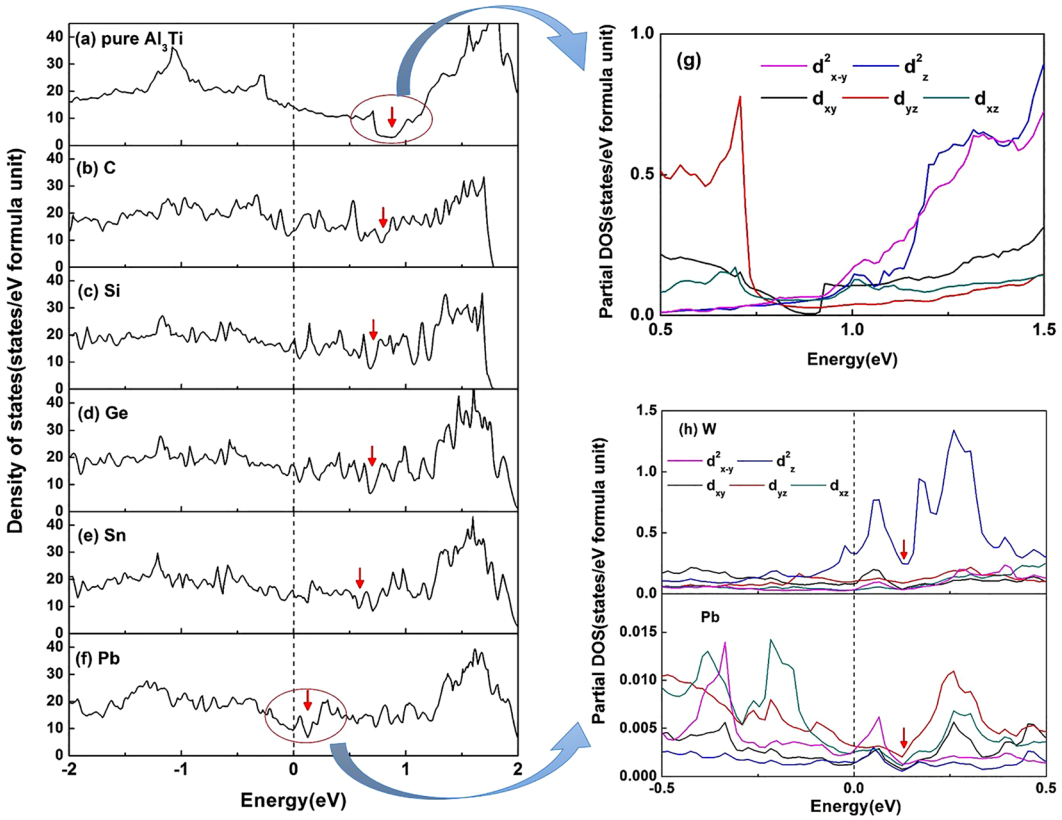


**Figure 3.** The calculated (DOS) of (**a**) pure $D0_{22}$-$Al_3Ti$, (**b**–**f**) W − M co-doping $Al_3Ti$ with an Al vacancy at $V_1$ site, W = C, Si, Ge, Sn and Pb, respectively. The calculated partial DOS of (**g**) pure $D0_{22}$-$Al_3Ti$, (**h**) W-Pb co-doping $Al_3Ti$ (Note only 3d orbitals are presented here). All arrows indicate the psuedogap position.

level. The result is shown in Table 3. A clear pseudogap is observed in the $D0_{22}$-$Al_3Ti$ (circled part in Fig. 3a), which indicates the strong bonding-antibonding separation. The result shows a strong hybridization existing in the $D0_{22}$ structure as well as a strong directionality in bonding. Therefore, it is difficult to form the slip system in the tetragonal $D0_{22}$ structure and leads to brittleness. The partial DOS of $D0_{22}$-$Al_3Ti$ around the pseudogap was investigated, shown in Fig. 3g. From the edges of the gap, the splitting 3d orbitals could be observed clearly, thus, $b_{1g}$ ($d^2_{x-y}$) energy is higher than $a_{1g}$ ($d^2_z$) on the right edge, while $b_{2g}$ ($d_{xy}$) energy is higher than $e_g$ ($d_{xy}$, $d_{yz}$) on the left edge, which appears a typical tetragonal crystal field.

From Fig. 3b–f, by adding different M elements and forming a W − M co-doping cluster with an Al vacancy at $V_1$ simultaneously, the pseudogap migrates from far above towards the Fermi level, indicated by the red arrows.

| | C | Si | Ge | Sn | Pb | Al | Ti | W |
|---|---|---|---|---|---|---|---|---|
| $R_M$(Å) | 0.16 | 0.4 | 0.53 | 0.69 | 0.78 | 0.39 | 0.42 | 0.66 |
| EN | 2.50 | 1.74 | 2.02 | 1.72 | 1.55 | 1.47 | 1.32 | 1.40 |

**Table 4.** Ionic Shannon radius[24] ($R_M$) and the electronegativity (EN)[25].

The results show that there are less bonding states which may favor a $D0_{22}$ to $L1_2$-like transition. To carry out a more in-depth and detailed study, partial DOS crossing the pseudogap of the W-Pb co-doping system was calculated and shown in Fig. 3h. Contributions from W and Pb to bonding electrons were investigated separately. On the right edge of the pseudogap, it is observed that W-atom contributes a lot to form strong hybridization between the $d^2_z$ and $d^2_{x-y}$ levels. Similarly on the left edge of the pseudogap, the Pb-atom has a strong influence on rising the $d_{xz}$ energy and $d_{yz}$ energy towards the $d_{xy}$ level (or a strong hybridization among these 3d orbitals). Therefore, the vacancy-induced 3d-orbital-splitting tend to facilitate a ductile $L1_2$-like structure, thus, $e_g$ ($d^2_{x-y}$, $d^2_z$) and $t_{2g}$ ($d_{xy}$, $d_{xz}$, $d_{yz}$).

To obtain the brittle to ductile transition, the tetragonal $D0_{22}$ structure is expected to transform into an octahedral-like structure, which could be realized by either a shrinking along z-axis or an expanding on the xy-plane or both. By representing the ratio *r* of z-axis d to the xy-plane S, the change in structures are quantified, as shown in Fig. 2b. Taking pure $D0_{22}$-$Al_3Ti$ as the standard, it can be concluded that *r* decreased with the formation of Al vacancy at $V_1$ site, which indicates that the tetragonal crystal field tends to transform into an octahedral-like crystal field. As a result, the stable phase change from $D0_{22}$ to $L1_2$–like ductile structures. When an Al vacancy forms at the $V_2$ site, S remains nearly a constant except for the W-C co-doping. The larger S in the W-C co-doping system is due to the small size of C. Among all M elements in Table 4, C is the only dopant whose size is smaller than that of Al (0.39 Å for $Al^{3+}$). More details will be outlined in Session 3 below.

## Discussion

In order to enable a brittle to ductile transition, we proposed and validated a W − M co-doping mechanism to (1) generate sufficient Al vacancies in $D0_{22}$-$Al_3Ti$, and (2) simultaneously to manipulate specific electron energy levels to approach the high symmetry octahedral-like electronic structures. In particular, an equation for the lattice energy of W − M co-dopants is derived based on the $E_{W-M}$ (eV) given in Table 1:

$$E_{W-M} = -170.3 + 9.44R_M^2 \tag{6}$$

where $R_M$ is the ionic radius of M.

The calculated $E_{W-M}$ based on equation (6) is −170.1, −168.7, −167.6, −165.8, −164.6 eV for M = C, Si, Ge, Sn and Pb respectively, which is very close to the DFT calculations, thus, −169.9, −168.7, −167.9, −165.8, −164.6 eV. Therefore, $E_{W-M}$ is in proportional to the cross-session of an M-ion ($R_M^2$), or $E_{W-M}$ is 2-dimensional size (or xy-plane) dependent only. This is a good indicator that a W − M co-doping may only manipulate the xy-plane while leaving out the z-direction untouched.

Similarly, an equation for the formation energy of $V_2$-W − M co-dopants is derived based on the $E_{V_2}$ (eV) data given in Table 2:

$$\text{For Al−rich: } E_{V_2} = -3.9(R_M - 0.39)^2 \tag{7}$$

$$\text{For Ti − rich: } E_{V_2} = -0.55 - 3.9(R_M - 0.39)^2 \tag{8}$$

Both equations (7) and (8) reasonably reproduce DFT calculations shown in Table 2. We derived $V_2$-W − M equations only since they are stable (or having negative formation energy) for all the M elements. Like equation (6), both equations (7) and (8) are in proportional to the cross-session changes of a substitutional M-ion and an Al vacancy $(R_M - 0.39)^2$. Once again, a $V_2$-W − M co-doping may only manipulate the xy-plane while leaving out the z-direction untouched. This 2-D manipulation function of W − M co-doping is the basis that enables a brittle ($D0_{22}$) to ductile ($L1_2$-like) transition, which can be applied not only for $Al_3Ti$ but all intermetallics in general.

Finally, we have systematically investigated a series of W − M co-doping $D0_{22}$-$Al_3Ti$ (M = C, Si, Ge, Sn and Pb) intermetallics using first-principles calculation method. The site preference of W in pure $D0_{22}$-$Al_3Ti$ was first studied, it shows W (a *d* element) has a clear preference to substitute $Al_1$ (a *sp* element) site due to the strong crystal field. Then, we confirmed the $[(Al_{23}W)Ti_8]$ system is conductive to the subsequent doping of M-atom. Meanwhile, a M substitution of Ti reduces the stability of $[(Al_{23}W)Ti_8]$, which might benefit the intercalation and deintercalation of Al-ion during charge-discharge cycling in rechargeable Al-battery. The two possible Al vacancies were also investigated. In comparison to the vacancy formation energies of Li-ion in $Li_3N$[19] (−0.14 ~ 0.52 eV), the Al vacancies in W − M co-doped $Al_3Ti$ have much lower formation energies, therefore, high Al diffusivity is expected.

The DOS of W − M co-doping $Al_3Ti$ with an Al vacancy at the $V_1$ site were investigated. The results show the pseudogap migrates towards the Fermi level from far above, indicating a tendency to transform into ductile $L1_2$-like structure. By analyzing the partial DOS around the pseudogap, we found that W and Pb have almost independent contributions to the transition, thus, W mainly influents $d^2_{x-y}$ and $d^2_z$ while Pb have a strong effect on $d_{xy}$, $d_{xz}$ and $d_{yz}$. It shows the crystal splitting effect on the 3d orbitals plays a decisive role not only on the

formation but also the transformation of pseudogap. Therefore, this study contributes to the formation of a new field in physics to design mechanical properties from electronic structures via vacancy optimization.

## Methods

Calculations were carried out within the framework of density functional theory (DFT)[20], using the projector-augmented wave (PAW) method[21] and the Perdew-Burke-Ernserhof (PBE)[22] for the exchange-correlation energy functional, via the Vienna ab initio Simulation Package (VASP)[23]. We first calculated the equilibrium lattice parameters of the $Al_3Ti$ using plane-wave cutoff energy of 340 eV and a $7 \times 7 \times 7$ k-point mesh in the Monkhorst-Pack scheme[13] by using the $2 \times 2 \times 1$ supercell including 32 atoms. In all calculations, self-consistency was achieved with a tolerance in the total energy of 0.01 meV, and the atom were relaxed until the forces were less than 0.01 eV/Å. The crystal structures were fully optimized by independently modifying lattice parameters and internal atomic coordinates.

**Data availability statement.** All data generated or analyzed during this study are included in this published article.

## References


1. Jang, D. C. & Greer, J. R. Transition from a strong-yet-brittle to a stronger-and-ductile state by size reduction of metallic glasses. *Nature Mater* **9**(3), 215–219 (2016).
2. Peterlik, H. *et al*. From brittle to ductile fracture of bone. *Nature Mater* **5**(1), 52–55 (2006).
3. Ramos, L. *et al*. Structural signature of a brittle-to-ductile transition in self-assembled networks. *Phys. Rev. Lett*. **107**(14) (2011).
4. Tallinen, T. & Mahadevan, L. Forced tearing of ductile and brittle thin sheets. *Phys. Rev. Lett*. **107**(24) (2011).
5. Yuan, C. C. *et al*. NMR Signature of evolution of ductile-to-brittle transition in bulk metallic glasses. *Phys. Rev. Lett*. **107**(23) (2011).
6. Wu, P. & Wu, T. Temperature-dependent modulus of resilience in metallic solids – calculated from strain-electron-phonon interactions. *J. Alloys Compd*. **705**, 269–272 (2017).
7. Pan, Y. *et al*. Vacancy induced brittle-to-ductile transition of $Nb_5Si_3$ alloy from first-principles. *Mater. Des*. **86**, 259–265 (2015).
8. Yuan, Z. P., Cui, H. B. & Guo, X. F. First-principle calculation on mechanical and thermal properties of B2-NiSc with point defects. *J. Semicond*. **38**(1), 5 (2017).
9. Niu, H. Y. *et al*. Extra-electron induced covalent strengthening and generalization of intrinsic ductile-to-brittle criterion. *Sci. Rep*, **2** (2012).
10. Pan, Y. *et al*. Influence of vacancy on structural and elastic properties of $NbSi_2$ from first-principles calculations. *Mater. Des*. **108**, 13–18 (2016).
11. Shi, T. T. *et al*. Atomic diffusion mediated by vacancy defects in pure and transition element (TM)-doped (TM = Ti, Y, Zr or Hf) L1(2) $Al_3Sc$. *Mater. Des*. **108**, 529–537 (2016).
12. Hong, T. *et al*. Crystal-structure, phase-stability, and electronic-structure of Ti-Al intermetallics-$TiAl_3$. *Phys. Rev. B*. **41**(18), 12462–12467 (1990).
13. Milman, Y. V. *et al*. Mechanical behaviour of $Al_3Ti$ intermetallic and $L1_2$ phases on its basis. *Intermetallics* **9**(9), 839–845 (2001).
14. Chen, Z. L. *et al*. Chemical bonding and pseudogap formation in D0(22) and L1(2) structure (V, Ti)$Al_3$. *J. Phys. Chem. Solids*. **71**(7), 946–951 (2010).
15. Frazier, W. E. & Benci, J. E. Crystal structure and phase relationships in as-cast and melt spun $Al_3Ti$ and $Al_3Ti$ plus copper. *Scripta. Mater*. **25**(10), 2267–2272 (1991).
16. Ghosh, G. *et al*. Stability and elastic properties of $L1_2$-$(Al,Cu)_3(Ti,Zr)$ phases: Ab initio calculations and experiments. *Intermetallics* **15**(1), 44–54 (2007).
17. Wei, X. P. *et al*. The electronic and magnetic properties of defects on half-metallic $Ti_2NiIn$ alloy. *J. Solid State Chem*. **233**, 221–228 (2015).
18. Li, J. *et al*. First-principles study of Al/$Al_3Ti$ heterogeneous nucleation interface. *Appl. Surf. Sci*. **307**, 593–600 (2014).
19. Wu, S., Dong, Z. & Wu, P. Effect of transition metal (M = Co, Ni, Cu) substitution on electronic structure and vacancy formation of $Li_3N$. *J. Mater. Chem*. **21**(1), 165–170 (2010).
20. Loo, F. J. J. & Rieck, G. D. Diffusion in the titanium-aluminum system inter-diffusion between solid Al and Ti or Ti-Al alloys. *Acta. Metall*. **21**(1), 61–71 (1973).
21. Srinivasan, S., Desch, P. B. & Schwarz, R. B. Metastable phases in the $Al_3X$ (X = Ti, Zr, and Hf) intermetallic system. *Scripta Mater*. **25**(11), 2513–2516 (1991).
22. Kohn, W. & Sham, L. J. Self-consistent equations including exchange and correlation effects. *Phys. Rev*. **140**(4A), A1133–A1138 (1965).
23. Sridharan, S. & Nowotny, H. Studies in the ternary system Ti-Ta-Al and in the quaternary system Ti-Ta-Al-C. *Z. Metallkd*. **74**, 468–472 (1983).
24. Shannon, R. D. Revised effective ionic radii and systematic studies of interatomic distances in halides and chalcogenides. *Acta Crystallogr*. **32**(5), 751–767 (1976).
25. Allred, A. L. & Rochow, E. G. Electronegativities of carbon, silicon, germanium, tin and lead. *J. Inorg. Nucl. Chem*. **5**(4), 269–288 (1958).


## Acknowledgements

The authors acknowledge the computational resources from the National Supercomputing Center in Tianjin (TH-1A system). P. Wu's work on mechanical modeling is partially supported by the National Research Foundation, Prime Minister's Office, Singapore, under its Marine Science Research & Development Programme (Award Number MSRDP-P28).

## Author Contributions

M.K.Z., P.W., X.B. and Q.L.L. designed and coordinated the overall study. M.K.Z. and P.W. wrote the manuscript. Z.M.K. performed theoretical calculations with the help from P.W., X.B. and Q.L.L. All contributed to the discussions of the results.

## Additional Information

**Competing Interests:** The authors declare that they have no competing interests.